applied sciences

MDPI

Article

Energy Prediction and Energy Management in Kinetic Energy-Harvesting Wireless Sensors Network for Industry 4.0

Alex Mouapi [1,*] and Hatem Mrad [2]

[1] Department of Industrial Electronics at the Cegep of Abitibi-Temiscamingue, 425 BlVd. du Collège, Rouyn-Noranda, QC J9X 5E5, Canada
[2] School of Engineering, University of Quebec in Abitibi-Temiscamingue, Rouyn-Noranda, QC J9X 5E4, Canada; hatem.mrad@uqat.ca
* Correspondence: alex.mouapi@cegepat.qc.ca

Featured Application: The work proposes a new approach to design autonomous wireless sensor network based on kinetic energy harvesting.

Abstract: Real-time control and monitoring are some of the main goals of Industry 4.0. To meet these requirements, sensors are needed at every step of the production process. Wireless sensors (WS) are better suited due to their flexibility but are limited in energy. In this work, kinetic energy harvesting using piezoelectric technologies are considered to ensure the energy autonomy of a Wireless Sensor Network (WSN). First, unlike most existing works, this paper focuses on WSN rather than a single WS since the control of the entirety of most industrial processes requires several WSs. The solution proposed here is based on deep learning of the harvestable power signals at each sensor deployed on the monitoring system. Specifically, vibration measurements were performed at 12 locations on an ore crushing mill in a mine. From there, a mechanical–electrical conversion model considering the system's dynamics was set up to evaluate the power profile each of the WSs can harvest. Considering that the harvestable power has many peaks due to the different operating states of the engine, we first proposed a Predictor of the Harvestable Power from Vibrations (PHPV). Using a large database, compared to a state-of-the-art predictor, the Predictor of the Harvestable Energy from vibrations (PHEV) allows for significantly reducing the Root Mean Square Error (RMSE). More specifically, the lowest reduction achieved for RSME ranged from 9.4 µW (with PHEV) to 5.9 µW (with PHPV). A decrease in RMSE ranging from 18.45 to 4 µW was obtained for another measurement point. Since harvest rates differ from one location to another, a Hierarchical Energy-Balancing Protocol (HEBP) is proposed to maximize the number of WS capable of transmitting information about the system's state, thus avoiding an interruption of the network coverage. In the HEBP, it is envisaged that some WSs, besides transmitting data, will supply other nodes with an energy deficit to allow them to communicate information about their location. For a minimum packet size of up to 1100 bits, the energy autonomy of all the WSs is ensured, unlike only 66% of the nodes with the previous protocols.

Keywords: Industry 4.0; vibration; energy harvesting; energy prediction; WSN; PHPV; PHEV; HEBP

Citation: Mouapi, A.; Mrad, H. Energy Prediction and Energy Management in Kinetic Energy-Harvesting Wireless Sensors Network for Industry 4.0. *Appl. Sci.* **2022**, *12*, 7298. https://doi.org/10.3390/app12147298

Academic Editor: Junseop Lee

Received: 22 June 2022
Accepted: 19 July 2022
Published: 20 July 2022

1. Introduction

In the fourth industrial revolution, machines must communicate autonomously to optimize processes. It emerges from the previous literature that the hallmarks of Industry 4.0 are intelligent automation and the integration of new technologies [1]. To have these characteristics, the basic elements of Industry 4.0 are real-time communication and the possibility of making systems communicate with each other and humans. Industry 4.0, therefore, emphasizes digital technology and ubiquitous connectivity. The devices for establishing communication are sensors, and these can be wired or wireless. Connectivity is achieved by using a network of sensors. Wired sensors require a cable for their power

supply and data transmission. This makes them less flexible in deployment. Wireless sensors (WS) are more flexible, space-saving, have a low cost, are quite robust, and have little impact on the environment [2]. Due to these many advantages (especially flexibility), the WSs adapt better to the requirements of Industry 4.0. Despite this flexibility, one of the main constraints in deploying WSs is the energy limit, due to the limited size of their battery [3]. Thus, although Industry 4.0 envisages that machines can communicate with each other autonomously, the fact remains that this objective can be achieved if WSs are also guaranteed energy autonomy.

1.1. Context and Problem Definition

The above justifies the need for WS to meet Industry 4.0 objectives. However, the issue of energy limitation causes many problems because battery-charging solutions can be expensive (since they very often involve a cessation of production) and can sometimes be impossible when the WS is deployed in places that are difficult to access. To overcome this limitation, a field of research has been expanding in recent years; it is that of ambient energy harvesting [4], which consists of targeting an ambient source (heat, light, vibration, electromagnetic signals, etc.) around the sensor and convert it into appropriate electrical energy. This work is then part of the context of ambient energy harvesting to ensure the energy autonomy of the WS. The vibrations generated by the actuators are the primary energy source considered.

Note that, unlike battery-powered WS, one of the limitations (regardless of the primary power source) in Energy Harvesting WSs (EH-WS) is the fluctuating nature of harvestable power. In solar energy harvesting, this is due to the alternation of day/night and the change of seasons. Radiofrequency waves, for example, are vulnerable to the propagation channel between the emitting and receiving source, which is often dynamic. The primary energy source considered in this paper is vibration. Most vibration signals will exhibit many fluctuations that depend on the operating regimes of the machines that generate these vibrations [5]. It should be noted that regardless of the industrial process, the engine will be either empty or under full load and even overloaded at a given time. This fluctuating (sometimes random) nature of the harvestable power makes it difficult to define the specifications of the autonomous WS. Yet, it is important to transmit information at regular intervals to every controlled location on the monitored system. This will prevent the loss of information due to a data queue.

On the other hand, predictive maintenance is also one of the requirements of Industry 4.0, and to effectively control an industrial process, a significant amount of operational data is required. For example, in the same industrial process, accelerometers can be used to measure vibration levels at the reducers, temperature sensors are useful to measure the heating of conductors due to current passages in an engine, pressure sensors can be used during lubrication processes, etc. These massive amounts of data, usually stored in the cloud [6], are not only used for maintenance operations but also for quality improvement. Thus, several sensors are necessary for the control of the entirety of an industrial process. However, much of the work proposed in recent years is only concerned with a single WS's energy autonomy. It is often the one located on the engine, which is where the harvestable amounts of energy are important. Ensuring a single sensor's energy autonomy, as is often the case, would not be enough to guarantee full control of an industrial process. Thus, two issues are addressed in this paper: the *fluctuating nature of the harvestable power* and that concerning the *efficient management of energy at the level of the Wireless Sensor Network* (*WSN*) and not of a single WS as in [7].

1.2. Related Work and Main Contribution

To answer the issue of the randomness of the harvestable power, two lines of research must be combined. This includes research in optimizing the performance of the harvesting circuits [8] and the efficient managing of the available energy [9]. Very little research, however, integrates these two aspects into their designs.

There are four main mechanisms for converting vibration into electrical energy in harvesting circuits. These mechanisms are electrostatic, electromagnetic, piezoelectric, and triboelectric. A comparison of these different transduction mechanisms has been proposed in [10–13]. It emerges from a synthesis of these previous works that piezoelectric materials are the most used due to their high output voltage and the facility of shaping the harvested energy. It should be noted that the transducer's performance is also determined by its geometry. To harvest the maximum power, the transducer's resonant frequency must match the surrounding vibrations' main frequency [14]. There are three main types: cantilever, circular, and cymbal-type transducers [15]. Given the low frequencies in most applications, cantilever beams are the most considered structures because they make it possible to reach low resonance frequencies while maintaining acceptable dimensions [15,16].

The major disadvantage of piezoelectric cantilever-type beams is their narrow bandwidth; however, most vibration spectra are wideband [16]. The optimizations are then mechanical in nature, using multi-beam harvesters to increase the transducer's bandwidth [17]. For example, in [18], five piezoelectric beams connected in series are used to harvest 66.75 μW for an acceleration of 5 m/s^2 at 234.5 Hz of frequency. Reconfigurable transducers are also being considered to overcome the fluctuation observed in most vibration spectra. The general principle of the technique is based on adjusting the proof mass of the cantilever beam. In [19], a stepper motor performed the proof mass adjustment. Although the results yielded a 60.56% bandwidth improvement with a conversion efficiency of 84.8%, the engine used to adapt the system consumed some of the harvested energy. In [20], the power harvested on the different axes was analyzed beforehand. The harvesting system's location was defined according to the level of harvestable energy. Although effective, these solutions were suitable for applications where the amounts of vibrations are important, since the adjustment systems consume a part of the harvested energy. Moreover, improvements on the mechanical level are achieved at the expense of the congestion generated by the circuits' size.

Electrical solutions are also proposed to amplify the power at the output of the piezoelectric transducer. For example, non-linear processing techniques to amplify the amount of power harvested have been proposed. Non-linear techniques consist of intermittently switching the piezoelectric transducer on a resonant electrical network for a short time [21]. The main method is the synchronized switch harvesting on the inductor [7]. Thanks to this technique, it is possible to amplify the transducer's output power and output voltage, but this is generally for a fixed excitation frequency [17], which is difficult to maintain in real applications. It has also been shown experimentally in [22] that these optimization techniques are only gainful when the transducer's open-circuit voltage is greater than 5.84 V; this is at a frequency of 30 Hz. It has nevertheless recently been proposed in [23] a reconfigurable nonlinear method, efficient for open-circuit voltage levels of the transducer between 0.03 V and 4.39 V. Although the simulated results of the proposed circuit demonstrated the efficiency of 66%, it remained that this performance was achieved by using several (up to 8eight piezoelectric transducers, which once again contributed to increasing the size of the circuits. In addition, the proposed solutions only consider optimizing the capacity of a single WS located at a predetermined location in the network. This does not guarantee that all WSs in the network can be self-sufficient as the expected energy harvest rate depends on the location of the WS. Unlike these previous studies, this paper first proposed to design a *Predictor of the Harvestable Power from Vibrations* (*PHPV*).

Regarding power management solutions, although many solutions have been proposed in recent years for battery-powered WSs, the possibilities in terms of EH-WS are still limited. Most energy management techniques proposed in the literature only concern a single harvester node [24,25]. The general method proposed uses ultra-low consumption components and the duty cycle strategy [26]. Since reducing the duty cycle is achieved by increasing the WS's sleep mode duration, most of the proposed solutions do not regard of the Quality of Service (QoS). For example, in [27], a WS equipped with a piezoelectric vibration harvesting system with a 0.33 pF supercapacitor could transmit data after 12 h.

In [24], for example, a PID (Proportional Integral Derivative) controller for measuring the difference between the energy harvested and the energy stored in the WS battery is designed to adjust the WS specifications at each measurement cycle automatically. In [25], the duty cycle adaptation strategy was used to enslave the performance of the WS to the capacities of a piezoelectric beam fed by the vibration of 0.15 g at 40 Hz. The results obtained in this work show that the WS can transmit data every minute.

A few solutions have nonetheless been proposed to efficiently manage energy in ambient energy-harvesting networks [28–30]. Most of these solutions are variants of the Low-Energy Adaptive Clustering Hierarchy (LEACH) protocol initially proposed in [31], intending to balance the energy expenditure of nodes powered by a battery. The initial version of the protocol suggests local data processing and a rotation of the cluster head (CH) at each measurement cycle. The cluster head's choice is based on each node's residual energy. Minimization of energy consumption is thus achieved by reducing the transmission range of each WS; this is achieved by local data processing. Since the work in [31], many variants of the LEACH protocol have been proposed, but always for battery-powered WSs. Some of the most important propositions are summarized in [32]. Only recently have some studies considered adapting the LEACH protocol to ambient energy-harvesting networks [28–30,33]. In [28], a CH selection scheme is proposed, and compared to the original LEACH; three types of WS coexisted in each cluster. These were the CH, the WS members, and a scheduling WS whose function is to record the residual energy of each WS. The role of the WS scheduler is to designate the cluster head at the start of the measuring cycle. In [28], the energy harvest rate for the current cycle was not considered; this resulted in a decrease in the QoS of the network, by increasing the delay in data transmission. In [29], authors used the same scheme as that of [28] with only two types of nodes in the cluster (the CH and the WS members). Again, the predictor was not built into the design, and QoS was defined under the basis of the available energy. In addition, the analyzes in [29] were based on solar power. In [33], a new adaptive clustered protocol for ambient energy harvesting WS was proposed. First, a hierarchy was established based on the network's energy level of the different WSs. The active phases of each WS were adapted according to the availability or not of the ambient energy, as in the case of the duty cycle strategy [26]. The proposed method makes it possible to ensure the perpetual operation of the network under the base of the harvested energy. However, the availability of data from the different WSs is not synchronous, thus making it difficult to make an intervention decision because it is often based on observing several physical quantities simultaneously.

Unlike most previous works, which only deal with the energy autonomy of a single WS, our study proposes a solution for optimizing the performance of a network of several WSs. The main goal was to ensure the energy autonomy of the WSN by giving all the WSs the ability to communicate regardless of their location in the industrial process. For this, a hierarchy of the different WSs of the WSN was established. This classification considers the residual energy and the expected energy harvest rate for each WS. After this classification, WSs with an energy deficit were powered by the WSs with an energy supplement. This allowed using the harvested energy to increase the data transfer rate of the whole WSN. Hence, this paper's second contribution consists of implementing a *Hierarchical Energy-Balancing Protocol* (*HEBP*). A conceptual view of the proposed protocol is presented in Section 4. The combined solutions (PHPV and HEPB) aimed to improves the network's QoS. The rest of the paper is organized as follows: Section 2 describes the design method and the tools used. In Section 3, we discuss the implementation of the proposed predictor (PHPV). Finally, Section 4 deals with the efficient management of harvestable energy with HEPB.

2. Design Method, Study Case, Objectives and Assumptions

2.1. Design Steps

In this section, the steps for setting up this work's two contributions are described and summarized in Figure 1, on which the main contributions are framed in blue. Firstly,

measurements of the acceleration signals at the various sensor locations were carried out as in [7]; the measurements were carried out throughout January 2022. The accelerometer used for the measurements was an ACC 103 accelerometer marketed by Omega Engineering. These accelerometers can record vibrations of up to 500 g for frequencies up to 10 kHz [34]. The vibration data were taken every minute, and then spectral analyzes were be carried out in the MATLAB environment. According to [35], this analysis will define the piezoelectric transducer's resonant frequency. A mechanical–electric conversion model considering the system's dynamics was then set up to analyze the harvestable power levels by the various sensors deployed in the industrial process. The PHPV was set up to minimize the root mean square error. Comparing the performance of PHPV with previous linear predictors completed this first step of the design method.

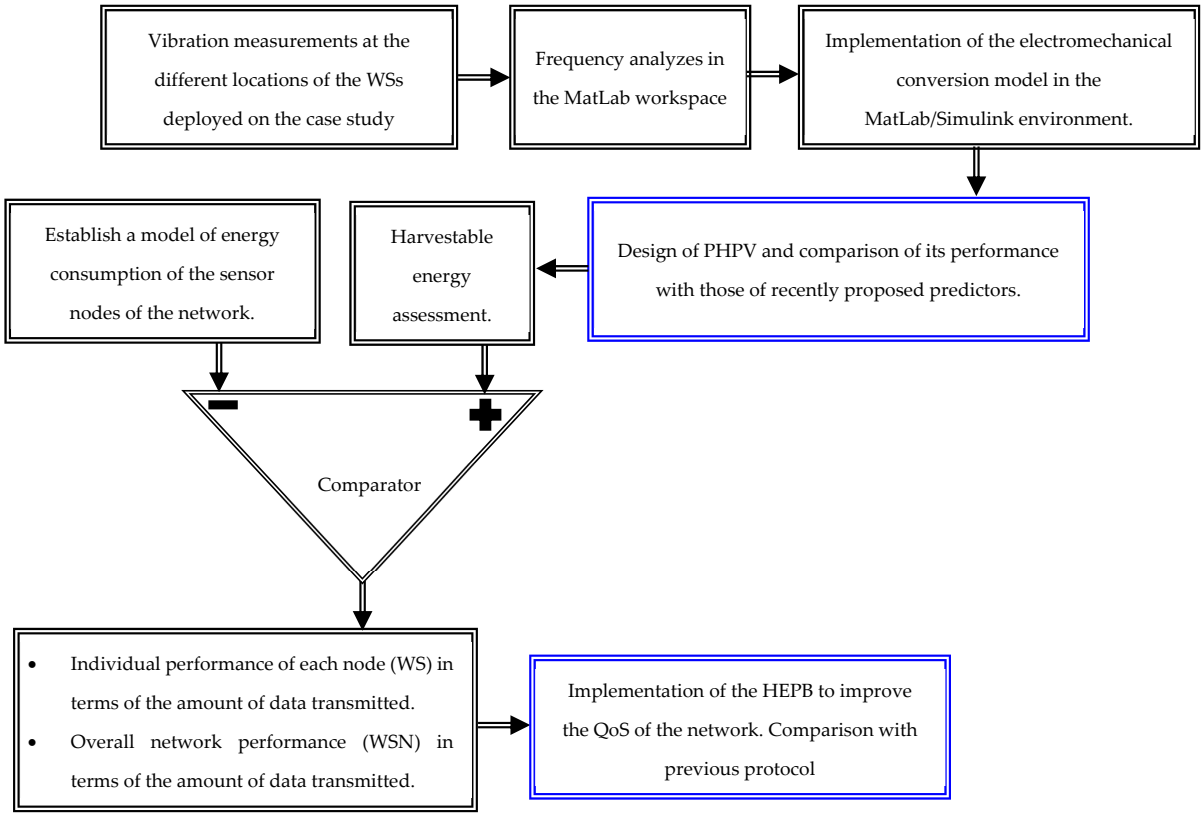

Figure 1. Different steps for the implementation of the PHPV and the HEPB.

For the implementation of the HEBP, an energy cost per data bit was established, and a comparison between the available energy (predicted by the PHPV) and the expenditure was carried out to define the quantity of data that can be transmitted at the end of the measuring cycle.

2.2. Network Model for HEBP Design

Once the ability to predict the amount of energy harvestable by each WS deployed on the system was effective, a minimum required QoS was defined. The network was partitioned into three WS groups, as shown in Figure 2 below. First, the highest harvest rate WS was designated as the CH node. In addition to collect data at its location, acts as a gateway between the other WSs and the BS. In a second step, energy assistance was envisaged between the other WSs of the network. As shown in Figure 2, there is energy assistance between the different WSs of the network. Based on the energy predicted by the PHPV, it was evaluated as to whether the WS has an energy greater than the required QoS; in this case, the WS is said to be self-sufficient. For a WS with less energy than the

required QoS, the WS was classified as needy and received energy from the self-sufficient WSs. Once the WS energy level balance is achieved, each WS transfers the collected data directly to the CH node. The CH node is the node whose residual energy added to the predicted energy harvest rate is the highest energy level in the network. The energy cost of the CH is then associated with the data reception, data aggregation, and data transmission to the Base Station (BS). The combined solutions (PHPV and HEPB) thus maximize the size of the data transmitted by each needy WS while improving the network's QoS through the number of WSs that can send information about the system's state.

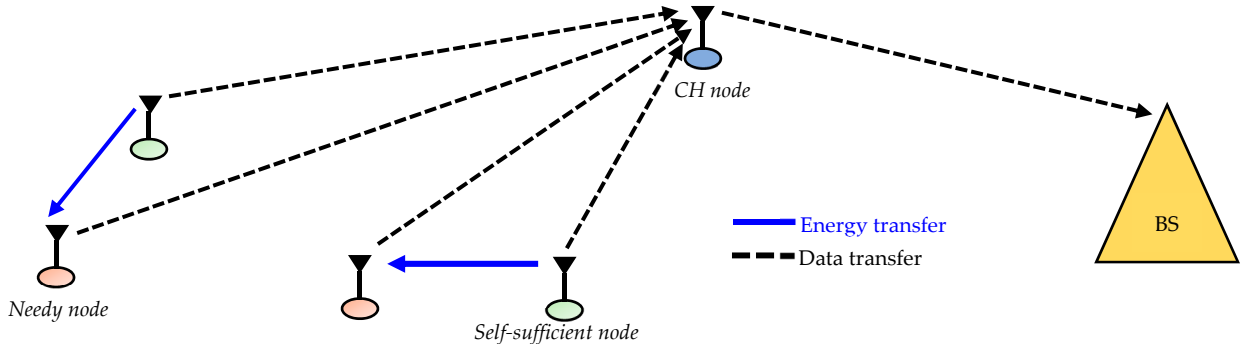

Figure 2. Energy assistance model between the different WS.

2.3. Study Case

In this paper, the network consisted of 12 nodes evenly distributed over the process to be controlled. The case study considered is part of the ore-crushing process at Agnico Eagle's Laronde mine. In this process, the ores must pass through two crushers. Two cyclones re-surround the minerals that have not been broken. For process monitoring, it is necessary to have many sensors, such as for speed, temperature, vibration (for shock analysis), pressure (for lubrication operations), etc. Our study was limited to the grinding diagram, shown in Figure 3.

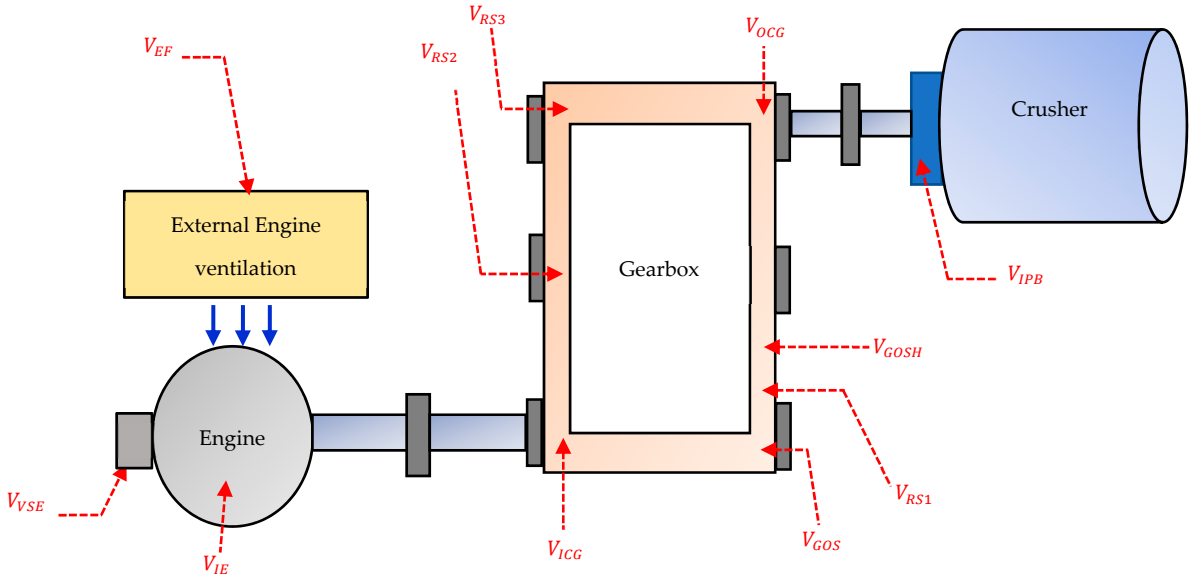

Figure 3. Study case and location of accelerometers on the SAG drive diagram.

This diagram shows a motor, Shaft 1, a speed reducer, Shaft 2, and a crusher from left to right. The figure also shows the measurement points where the accelerometers were placed. A description of these different measurement points and the terminology of

the different sizes that were considered throughout this paper is provided in Table A1 in Appendix A. Figure 4 shows a photograph of the accelerometer installed on the reducer.

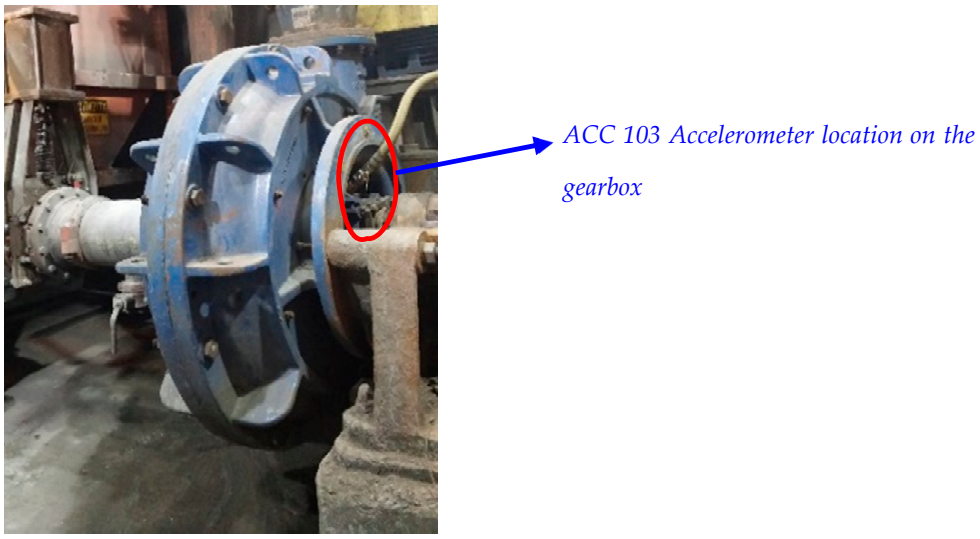

Figure 4. Accelerometers location on the gearbox.

2.4. Specific Objectives and Assumptions

Two objectives were pursued in setting up the PHPV; these are the minimization of the relative error and the minimization of the Root Mean Square Error (RMSE). Two objectives were also targeted for the HEBP; the first was to maximize the number of active WSs. The second objective was to increase the quantity of data transferred by each needy WS. To achieve these results, the following reasonable assumptions are considered throughout this work.

- Each WS in the network is equipped with a vibratory energy harvesting system and a wireless energy transfer/reception system [36].
- Data storage memory is assumed to be sufficient [7].
- The shaping of the energy harvested from the vibrations is not processed; it will be assumed that the WSs are equipped with maximum power point tracking [37].
- Linear behavior of piezoelectric transducers is assumed given the low vibration levels [38].
- The time division multiple access is considered to avoid interference when accessing the common radio channel [39].
- The gain of the channel between a needy WS and a self-sufficient WS is assumed to be unity.
- For the transfer of energy between the WS, time switching is considered; that is, the needy WS receives power for a fraction of time τT and transfers data during the other fraction of time $(1 - \tau)\ T$. T being the duration of a measurement cycle [40].
- QoS is characterized by the number of active WSs and the amount of data transferred to the BS.

3. Predictor of the Harvestable Power from Vibrations (PHPV) Design

3.1. Frequency Analysis and Mechanical-Electrical Conversion of the Vibration Signals

- To obtain the level of power for each WS deployed on the industrial process that can be harvested, we carried out a frequency analysis of the acceleration signals at the various locations of the accelerometers. The results are shown in Figure 5, and the used terminology is provided in Appendix A. The vibration peaks reached, as well as the corresponding frequencies, are indicated in the legend on each of the figures.

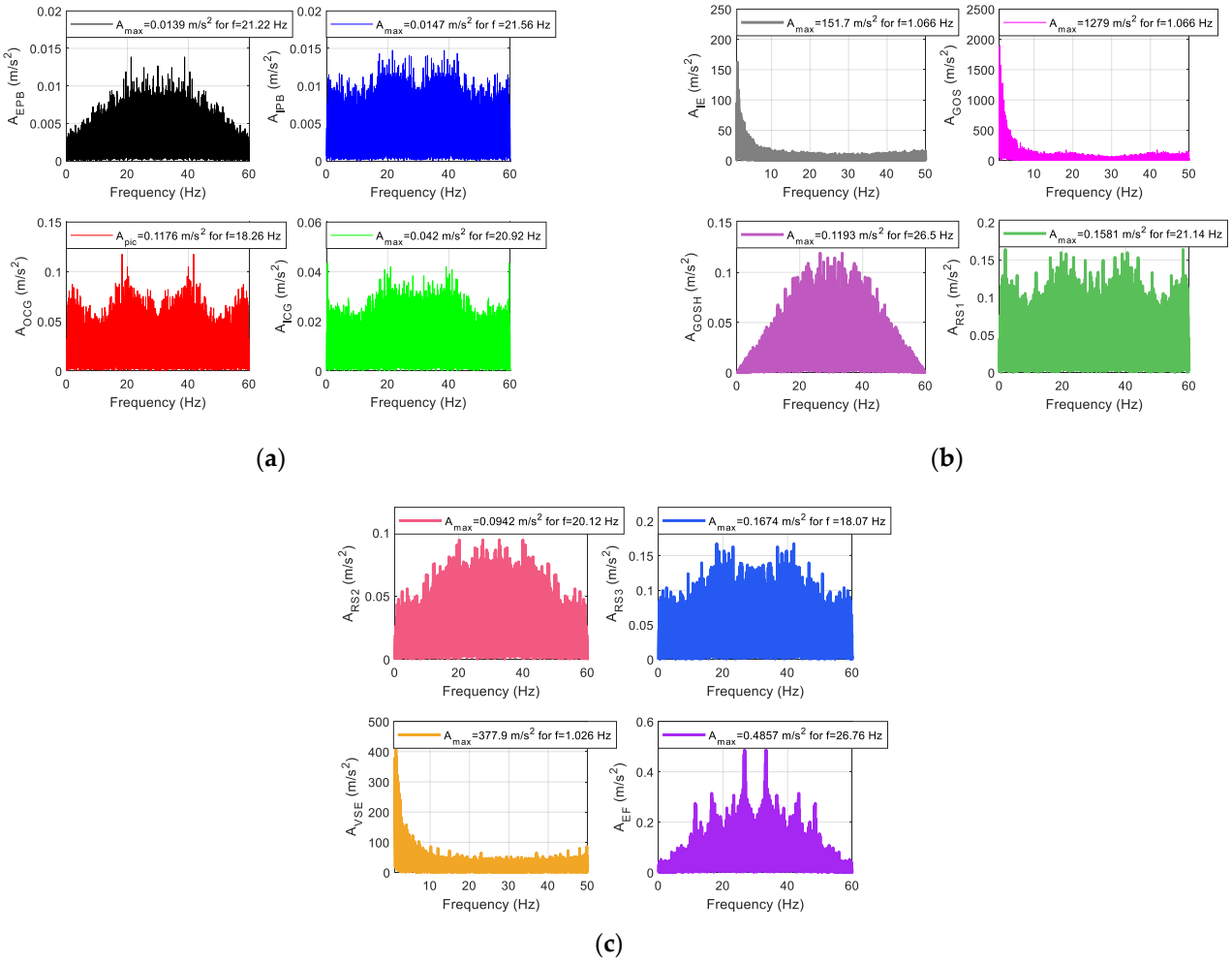

Figure 5. Frequency response of measured vibrations. (**a**) Vibrations on the crusher pinion (external and inside) and on the crusher gearbox (outlet and inlet). (**b**) Vibrations on the internal engine vibration, on the gearbox at the output side, on the gearbox output shaft and radial shaft 1. (**c**) Vibrations on the radial shaft 2, radial shaft 3, on the ventilation side of the engine, and engine fan.

The following observations emerge from Figure 5:

- The maximum acceleration values occurred at approximately the same frequency when the measurement concerned the same element (motor, gearbox, or crusher). For example, the maximum values occurred around 21 Hz for the measures concerning the crusher pinion, as shown in Figure 5a.
- The measurement campaign made it possible to identify four points with a low harvest rate: this is the level of vibrations at the outside the crusher pinion (black curve in Figure 5a); vibrations at the inside the crusher pinion (blue curve in Figure 5a), vibration at the outlet of the crusher gearbox (red curve Figure 5a) and vibration at the inlet of the crusher gearbox (green curve in Figure 5b).
- We also obtained three points with a high harvest rate which are the vibrations inside the engine (gray curve in Figure 5b), the vibrations at the level of the reducer on the output side (magenta curve in Figure 5b), and finally the vibrations at the level of the external ventilation of the engine (purple curve in Figure 5c).
- The acceleration peaks occurred at very low frequencies for measuring points with a high harvest rate. Although these low-frequency values contributed to obtaining high power levels, the fact remains that the appropriate transducers will also be bulky (this issue is not dealt with here).

- Overall, acceleration peaks occurred at low frequencies (less than 27 Hz) for all the measurement points. Thus cantilever-type piezoelectric transducers [15], which make it possible to reach low resonance frequencies while maintaining acceptable dimensions, would be appropriate for actual implementation.

Considering the measured vibration data, the mechanical–electrical conversion model is shown in Figure 6. This model is the same as what was considered in [7]. The measured vibration signal was first converted into a force signal using a Simulink-PS converter block. The generated force was determined using Newton's second law as follows:

$$F_i(t) = m_i \cdot A_i(t) \tag{1}$$

where $F_i(t)$ is the force applied at time t on the piezoelectric composite for location i, $A_i(t)$ represents the acceleration data measured at the different locations in the industrial process. Finally, m_i is the effective mass of the composite to achieve the desired resonance frequency. By specifying the resonance frequency in the parameterization of the piezoelectric composite, it calculates the value of the effective mass to achieve this frequency [41]. The piezoelectric composite was modeled by the Piezo Stack block from Simscape's Mechatronic Actuators library. The Piezo Stack block considers the system's dynamics through the damping factor ξ and the resonance frequency. Damping was considered by specifying the value of the mechanical quality factor Q_m in the dynamic forces tab [41]. The damping factor added to the R and C mechanical ports of the block is defined as follows:

$$\xi = \frac{\sqrt{mk}}{Q_m} \tag{2}$$

where m represents the effective mass of the transducer, which is calculated by the block using the resonant frequency value as mentioned above, and k is the short-circuit device stiffness.

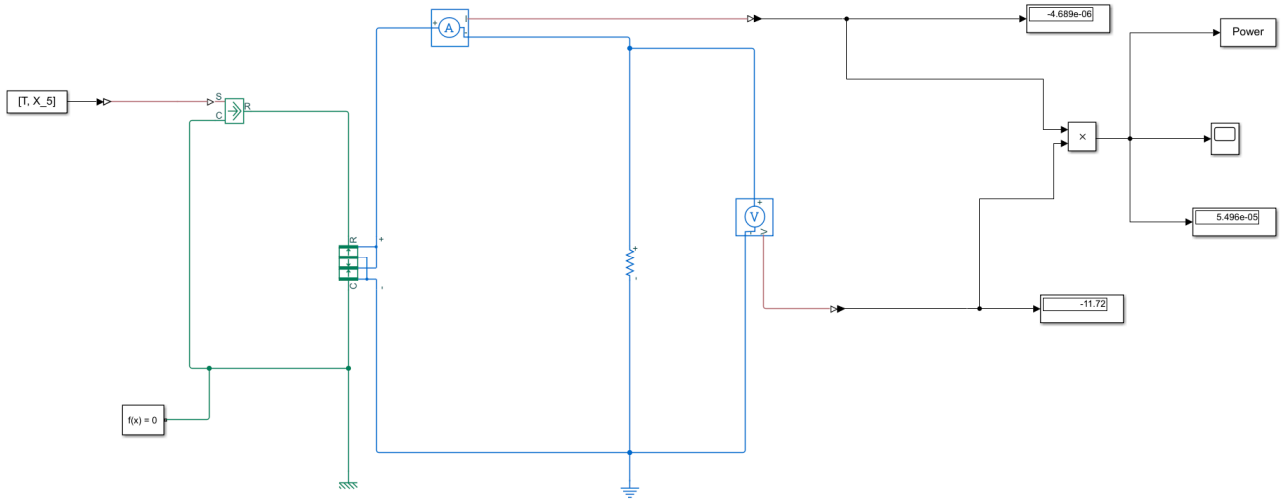

Figure 6. Mechanical–electrical conversion model of vibrations into electrical energy.

The values of the model's parameters of Figure 6 considered in this work are provided in Table 1. Most of the parameters used for the simulation come from the Midé Technology quick pack actuators datasheet [42]. The resonance frequencies' values were set to the different values captioned in Figure 5, depending on the measuring point. Note that the values of the model parameters can considerably influence the amount of harvestable power, but this is not relevant for the problem of the fluctuating nature of this power. For this reason, this issue is not addressed in this work. Using the parameter values in Table 1 and

the above model, the fluctuations in the harvestable power at the different measurement points are shown in Figure 7. The following findings emerge from these results:

- Numerous power peaks can be observed at each of the measurement points. These may be due to the different operating speeds of the engine, which generates the vibrations. Note that the engine can be empty (during loading), at full load (after loading) and sometimes overloaded or underloaded in the event of failure or wear of one or more teeth in the crusher.
- There is also (as expected) a hierarchy regarding the amount of energy harvested by the different nodes. For example, low harvest rate points exhibit power peaks of up to 5 µW, while for high harvest rate points, up to 49 mW are achieved, as is the case for vibrations at the output side reducer (magenta curve in Figure 7b). It would then be interesting to better exploit these different power peaks to predict them with good precision. This is the objective of Section 3.3, but before that, it is recalled in Section 3.2 for a brief state-of-the-art on energy prediction.

Table 1. Values of the model parameters for estimating the harvestable power.

Parameter	Value and Unit
Stack area	2.353 in^2
Stack length	1.81 in
Test voltage	20 V
No-load displacement at test voltage	0.04 mm
Blocking force at test voltage	500 N
Capacitance	125 nF
Resonant frequency at constant field	Values labeled in Figure 5
Mechanical quality factor	80
Load resistance	2.5 kΩ

3.2. Brief State of the Art on Linear Power Prediction

Many studies have been proposed in recent years to predict the amount of power harvestable from ambient energy sources [7,43–46]. Most of the proposed methods relate to solar energy, given the ease of access to the database of meteorological stations in different regions. The proposed methods are centered on the EWMA predictor [47]. The EWMA method defines a data sampling period [45]. More specifically, in [45], it considered data of the sun over seven days, and the observations were made every 30 min, corresponding to 48 time slots per day. The prediction method is based on the fact that on a typical day, the harvestable energy is similar to that harvested during the same time the previous day. Thus, the prediction of the harvestable power at the time t of day d, $\hat{p}_d(d,t)$ is defined in [45] as follows:

$$\hat{p}_d(d,t) = \alpha \hat{p}_d(t-1) + (1-\alpha) p_{d-1}(t) \quad (3)$$

where $\hat{p}_d(t-1)$ is the estimated power for the previous period, and $p_{d-1}(t)$ is the power harvested during the same period in the previous day; α is a weighting factor. For different values of α, the prediction error is evaluated, and the optimal weight is obtained as being that which minimizes this error. In [45], an optimal weight of 0.5 was obtained corresponding to an error in the output current of a solar panel of 2.3 mA. As we can see, in this method, the evaluation of the power is based on an estimate of the power in the previous time slot, which contributes to an increased prediction error. However, an advantage of the method, as proposed in [45], lies in the fact that it does not require a high storage space.

To improve the performance of the predictor, as defined in [45], the power at time t of day d, $\hat{p}_d(d,t)$ was estimated in [7,43,44] as follows:

$$\hat{p}_d(d,t) = \alpha p_d(t-1) + (1-\alpha) p_{d-1}(t) \quad (4)$$

with $p_d(t-1)$, which represents the real power harvested during the previous time slot for the current day; the other terms are the same used in Equation (3). In Equation (4), the

estimated power is determined using actual power data only, contrary to the algorithm proposed initially in Equation (3). This modification then contributes to minimizing the prediction error. While comparing the performance achieved with this algorithm defined by Equation (4) with that of other predictors described below, a prediction error of 33.26% was achieved for solar data recorded over 10 days in [43]. In [45], a prediction error of 28% was reached for solar data recorded over a year. Finally, using the vibration data recorded on the same process considered here, a relative error of 25.25% was achieved in [7].

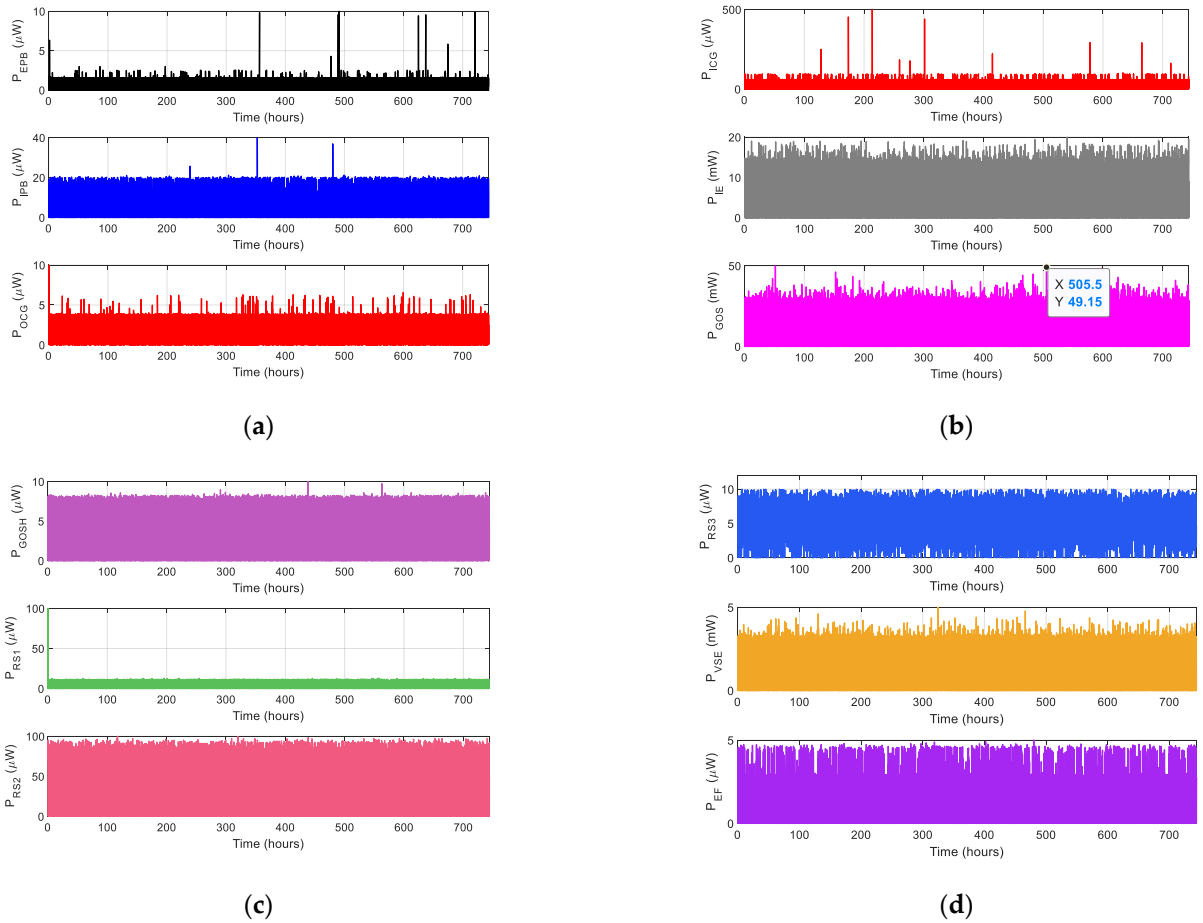

Figure 7. Fluctuations in the harvestable power at the different measuring points. (**a**) Harvestable powers on the Crusher Pinion and Crusher Gearbox (outlet). (**b**) Harvestable power on the Crusher Gearbox (Inlet), Internal Engine and Gearbox at the Output Side. (**c**) Harvestable power on the Gearbox Output SHaft, Radial Shaft 1 and Radial Shaft 2. (**d**) Harvestable powers on the Radial Shaft 3, Ventilation Side of the Engine and Engine Fan.

To improve the performance of the predictor defined by Equation (4), the model in [43] was proposed and known as the Weather-Conditioned Moving Average (WCMA). The model considers solar data from previous days and estimates solar power $\hat{p}_d(d,t)$ according to the algorithm below:

$$\hat{p}_d(d,t) = \alpha \cdot p_d(d,t-1) + (1-\alpha) GAP_k \cdot M_D(d,t) \quad (5)$$

where α is the weight of the filter defined in the same way as in [45]; $M_D(d,t)$ is the average of the power over the last D days at slot t; finally, the factor GAP_k measures the deviation between current solar conditions and previous days. The proposed method yields an average relative error of only 10%. However, it requires many calculations, which can cause delays in decision-making. In addition, to store the data obtained during the previous time

slots, the processor calculates the power gap each time; this can induce delays (depending on the processor's speed).

In [44], a new solar energy predictor designated by Solar Energy Predictor for Communicating Sensor (SEPCS) is proposed. The day is divided into 24 slots of time, and the power harvested during the time slot t is defined as:

$$\hat{p}(t) = \sum_{i=1}^{N_H} \alpha_i \cdot p(t-i) + \sum_{j=1}^{N_J} \beta_j \cdot p(t-24j) \quad (6)$$

where N_H is the number of hours in a day, $p(t-i)$ is the harvested solar power in the earlier N_H period intervals, N_J is the number of days considered in the database, and $p(t-24j)$ is the power harvested in the same time slot of the previous N_J days. α_i and β_j are the weights of filters with values between 0 and 1. This method uses a more extensive database than the EWMA algorithm; however, it is appropriate for slowly varying processes because the duration of a time slot was fixed at 30 min.

Recently, it has been proposed in [7] a Predictor of the Harvestable Energy from vibrations (PHEV). The method uses a more extensive database to reduce the RMSE from 28.63 to 19.52 mW when compared to the EWMA algorithm. The predicted power is expressed as follows:

$$\hat{p}_d\ (t,d) = \sum_{i=1}^{N_D} \alpha_i \cdot p_{d-i}(t) + \sum_{j=1}^{T} \left[\sum_{i=1}^{N_D} \beta_{i,j} \cdot p_{d-i}(t+j) + \sum_{i=0}^{N_D} \gamma_{i,j} \cdot p_{d-i}(t-j) \right] \quad (7)$$

where N_D represents the number of previous days, and T is the assumed periodicity observed in vibration signals due to repetitive tasks in the process. $p_{d-i}(t)$ is the harvested power in the previous days at the same moment t. $p_{d-i}(t-j)$ and $p_{d-i}(t+j)$ are, respectively, the powers harvested during previous days in earlier and successive periods. α_i, $\beta_{i,j}$, and $\gamma_{i,j}$ are weights of the filters. The database in this equation is huge, and this would require a lot of storage space. Taking multiple data into account when calculating power could also lead to a delay in decision-making. In addition, in this method, periodicity is considered in the vibration signals due to the habits of the process, which operates 24 h a day. However, it should be noted that this periodicity, assumed to be constant in the algorithm, could not remain so in an actual industrial application, because the wear of the equipment would influence the energy consumption profile of the engine, which would impact the characteristics of the acceleration signals [48]. These three observations taken together could then contribute to increasing the prediction errors.

In [46], a prediction based on machine learning of piezoelectric energy harvesting from wake gallop was proposed; the method does not deal with a real case but analyzes the vibration response of piezoelectric energy recuperators to wake gallop in different configurations. Once again, the actual implementation would be complex, given the wear and tear of the equipment.

3.3. Proposed Predictor

Since the industrial process operates seven days a week and 24 h a day, the data stored in the database was initially divided into days. Each time slot corresponds to one minute, as shown in Figure 8, where it is also highlighted the history of the data used to predict the harvestable power.

The predictor proposed in this work takes advantage of the results obtained in previous predictors. Since it has been shown in previous works that the EWMA method fails at the appearance of power peaks [7,44], to improve the precision in the estimation of the power, the gap between the estimated and actual power during the previous time slots was taken into consideration.

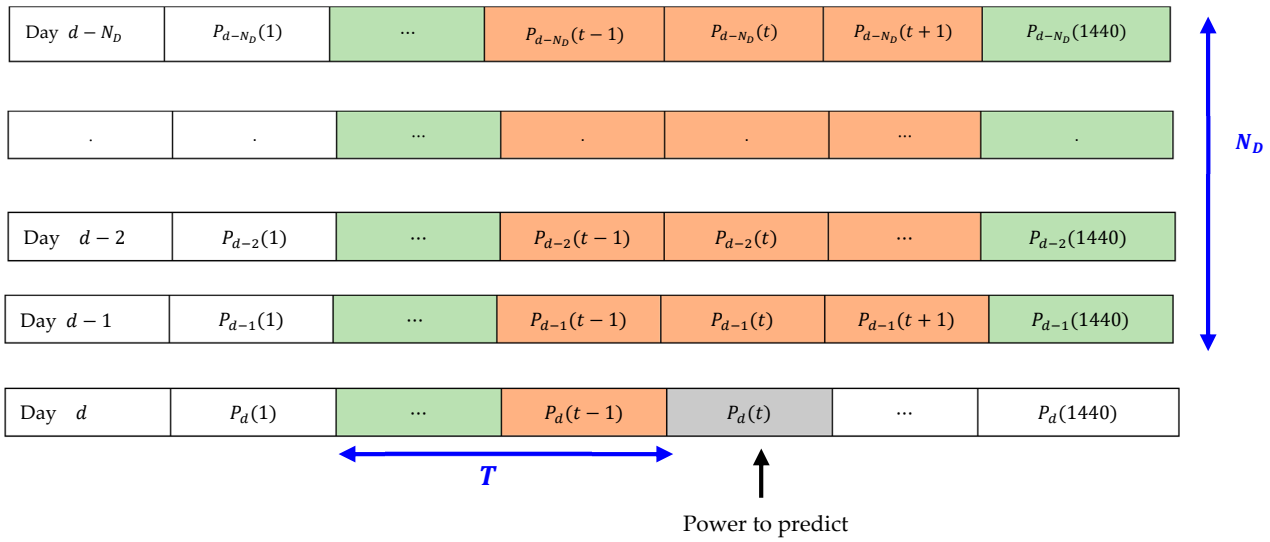

Figure 8. Database to PHPV design.

$$\hat{p}_d\ (t,d) = \sum_{i=1}^{N_D} \alpha_i \cdot p_{d-i}(t) + \sum_{j=0}^{N_D} \beta_j \cdot p_{d-j}(t-1) + \sum_{u=1}^{T} \gamma_u (p_d(t-u) - \hat{p}_d(t-u)) \qquad (8)$$

where $\hat{p}_d\ (t,d)$ represents the estimated power at time t of day d. N_D is the number of previous days taken into account in the estimate, and α_i, β_j, and γ_u are, respectively, the weights of the filters allowing consideration of the powers measured in the last days at the same time, that of the previous days at the earlier time slots and finally, and the gap between the powers measured and estimated during the previous time slots. Optimum weights were determined to minimize RMSE. T represents the number of slots, making it possible to optimize the prediction.

Using the algorithm defined by Equation (8), the optimal weight $(\alpha_{\text{opt}},\ \beta_{\text{opt}},\ \gamma_{\text{opt}})$ for each estimate was determined then the error was calculated to find the optimal value of T. The evolution of the RMSE for the vibration on the gearbox at the output side, according to T and N_D, is represented in Figure 9. The figure shows that the RMSE decreases with the number of days considered in the database. For all the curves, the optimal value of T is around 25; this value of T was used for the rest of the analyses.

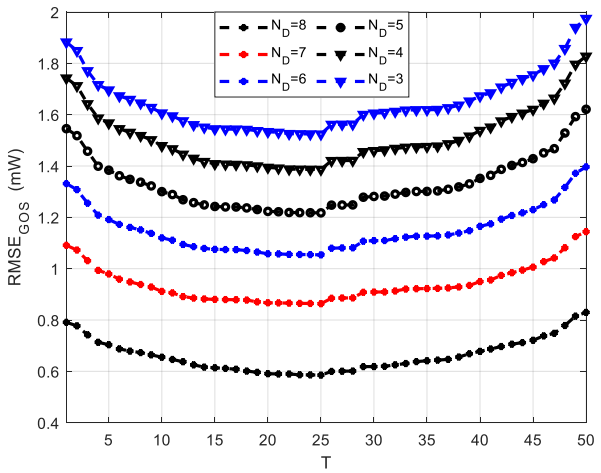

Figure 9. RMSE according to the number of the previous times slots T.

In the following, the performance achieved with the PHPV is compared with previous predictors, such as the EWMA defined by the algorithm in Equation (4) and the PHEV determined by the algorithm in Equation (7). The performance criteria considered in this paper are the maximum absolute error $E_{a_{\max_i}}$, and the RMSE $(RMSE_i)$, respectively defined as below:

$$\begin{cases} E_{a_{\max_i}} = \max(abs\ (p_i - \hat{p}_i)) \\ RMSE_i = \sqrt{\mathbb{E}(p_i - \hat{p}_i)^2} \end{cases} \tag{9}$$

where $\mathbb{E}$ is the expectation and p_i denotes the real power and $\hat{p}_i$, the predicted power.

The PHPV predictor's performance compared to those achieved with the EWMA and PHEV predictor is represented in Figure 10. For the twelve measurement points, the improvements obtained with the PHPV predictor compared to the PHEV predictor, about the relative error and the RMSE are reported in Table 2. For each measurement point shown in Figure 10, the representation is made around the most pronounced peaks, and the main observations are as follows:

- Compared to the EWMA (curve in black dotted line), we observed shifts in the appearance of the power peaks with the real power represented in solid black lines. This can give rise to an overestimation of the performance of a WS at a given instant and an underestimation of its performance at the next time slot.
- The signals predicted by the PHEV algorithm (in red) are more in phase with the real power in most cases. This can be explained by the fact that the algorithm, as defined in Equation (7), considers the time slots after the current time slots. However, there are considerable differences between the actual and predicted power. This discrepancy can be explained by the fact that the periodicity in the signals is shifted because of wear in the equipment.

Table 2. Comparison of EWMA and PVHE performance.

Measuring Points	Absolute Error			RMSE			
	EWMA	**PHEV**	**PHPV**	**EWMA**	**PHEV**	**PHPV**	**Improvement**
V_{EPB}	9.7 µW	5.1 µW	1.42 µW	0.6 µW	0.29 µW	0.08 µW	72.41%
V_{IPB}	34.4 µW	18.92 µW	5.34 µW	7.4 µW	2.9 µW	0.84 µW	71%
V_{OCG}	9.8 µW	2.6 µW	0.8 µW	1.7 µW	0.71 µW	0.22 µW	69%
V_{ICG}	440 µW	162.97 µW	116.8 µW	7.8 µW	9.4 µW	5.9 µW	37.2%
V_{IE}	6.7 mW	9.3 mW	2 mW	1.3 mW	3.27 mW	0.73 mW	77.6%
V_{GOS}	26.7 mW	24 mW	5.22 mW	3 mW	6.7 mW	1.5 mW	77.6%
V_{GOSH}	7.9 µW	4.92 µW	1 µW	2.4 µW	1.7 µW	0.37 µW	78.24%
V_{RS1}	55 µW	10.41 µW	6.77 µW	1.54 µW	1.77 µW	0.4 µW	77.4%
V_{SR2}	81.3 µW	49.09 µW	9.46 µW	26.5 µW	18.45 µW	4 µW	78.32%
V_{SR3}	6.8 µW	4.55 µW	1.42 µW	1.54 µW	1.53 µW	0.5 µW	67.3%
V_{VSE}	2.3 mW	1.94mW	0.55 mW	0.3 mW	0.62 mW	0.17 mW	72.58%
V_{EF}	4.9 µW	2.2 µW	0.6 µW	1.7 µW	0.71 µW	0.18 µW	74.65%

For all the measurement points, we first observed that the power predicted with the PHPV (blue curve) is more in phase with the real power. In addition, it is noted that considering the power difference during the time slots makes it possible to reduce the absolute error. To conclude this part, Table 2 summarizes the performance of the three predictors.

In Table 2, the RMSE is minimal with the PHPV when compared to the values reached with the EWMA and PHEV algorithms. Improvements range from 37.2% for vibrations taken at the inlet of the crusher gearbox to 78.32% for vibration signals measured from radial shaft 2. With this ability to calculate the quantity of harvestable power at each controlled location with the slightest error, a protocol is proposed in the following section to optimize the performance of the wireless sensor network.

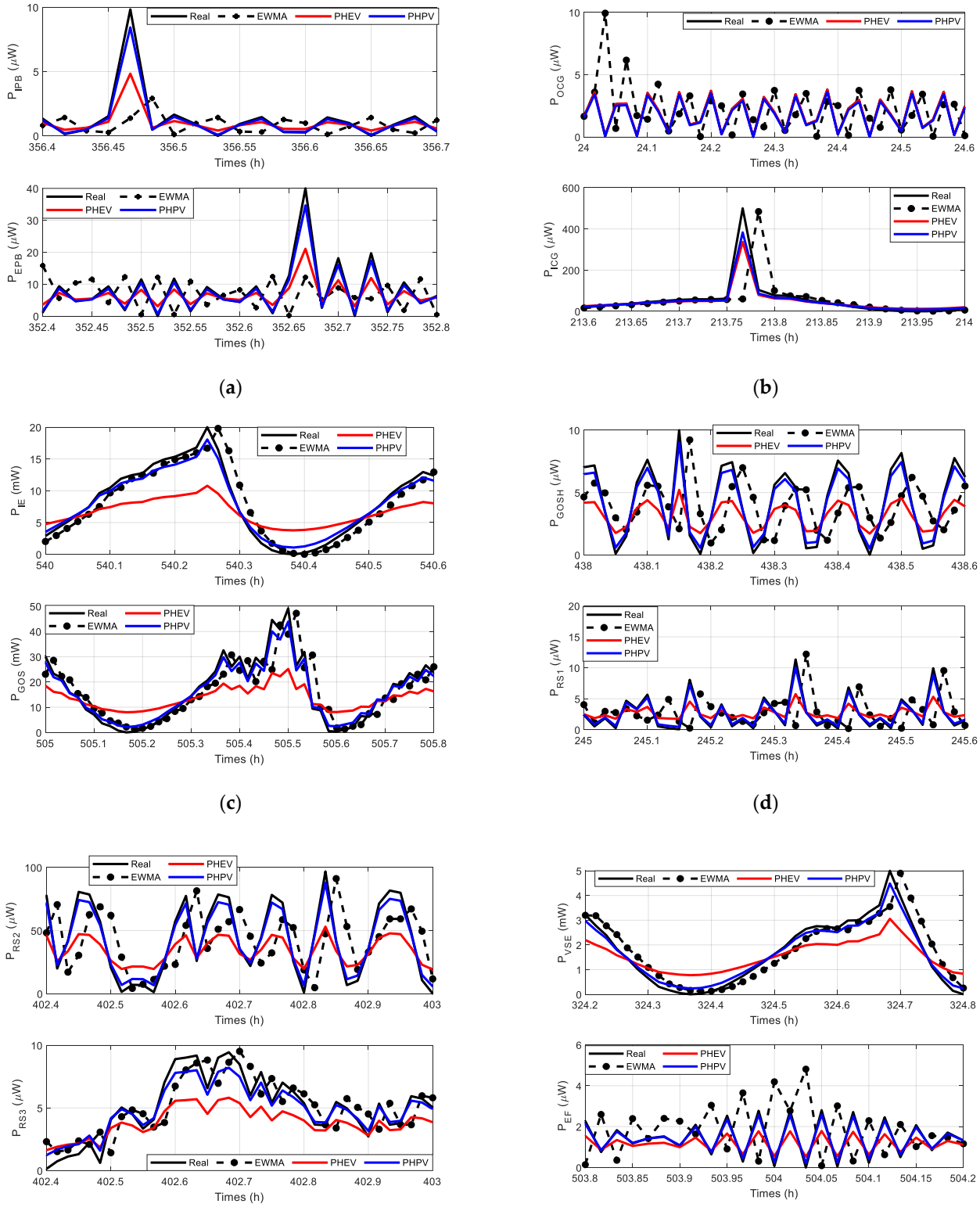

Figure 10. PHPV performance compared to EWMA and PHEV. (**a**) Power on External and Inside Crusher Pinion. (**b**) Power at the Outlet and Inlet of the Crusher Gearbox. (**c**) Power at Internal Engine and Gearbox at the Output Side. (**d**) Power on the Gearbox at the gearbox output Shaft and on the on the Radial Shaft 1. (**e**) Power on the Radial Shaft 2 and 3. (**f**) Power at the Ventilation Side of the Engine and Engine fan.

4. Hierarchical Energy Balancing Protocol (HEBP) Design

The results of the previous section suggested that some nodes had higher harvesting capacities than others; this can be observed in any industrial process. From this, it is evident that the WSs with a high harvest rate will have the capacity to transmit sufficient data, and the other nodes will not, for a fixed duration of the measurement cycle. However, in the control of an industrial process by several WSs, it is essential for a possible intervention that the data at the different measurement points are accessible simultaneously, hence the need to balance the energy level of the various nodes of the network. This is the objective of the proposed management method, which consists of implementing the HEBP in the network. The proposed protocol aimed to improve the WSN's QoS.

4.1. Quality of Service in WSN

QoS is one of the significant aspects of any application, and WS is therefore not spared. For WS, QoS reflects the sensor's ability to guarantee the performance required by the application [49]. QoS can be assessed through many aspects such as delay in data transmission, throughput, reliability, data accuracy, and network lifespan. By summarizing these different aspects, QoS can be assessed through the quantity and/or quality of data that can be transmitted. This work considers the capacity of the sensor nodes about the quantity of data that can be transferred to the BS. The other objective of the proposed protocol is to maximize the number of nodes that can transmit data at a given time.

Recall that in battery-powered wireless networks, QoS improvement is often achieved through energy efficiency optimization [50]. Energy-efficient management solutions aim to reduce the energy dissipation of the WS. In the case of ambient energy harvesting WSs, effective management consists of ensuring an Energy-Neutral Operation (ENO) at each WS [51]. The ENO condition is assured for node i when the harvested energy E_{H_i} remains greater than its energy expenditure E_{WS_i}. In most cases, this state is achieved by leaving the WS in standby mode for as long as possible, contributing to the deteriorating Quality of Service (QoS).

4.2. Performance Evaluation of Each WS Based on Its Harvesting Capacity

By setting a measurement cycle time of τ; corresponding to the frequency at which each WS must transmit information about the state of the system, the harvestable energy during a measurement cycle for node i is evaluated as follows:

$$E_{H_i} = \int_{t}^{t+\tau} \left(p_{PHPV}(u) - E_{a_{\max_i}} \right) du \tag{10}$$

where t is the start time of the measurement cycle, $p_{PHPV}(u)$ is the power predicted by the PHPV during the measurement cycle. As defined in Equation (9), $E_{a_{\max_i}}$ corresponds to the maximum absolute error reached; the values depending on the measurement points are reported in Table 2. An energy cost per bit E_{WS} was established, so the maximum quantity of bits that can be transmitted by node i, in a measurement cycle is the solution to the following optimization problem (designated by P1) [7]:

$$\min_{b} \left(E_{H_i} - b \cdot E_{WS} \right) \tag{11}$$

Subject to:

$$\begin{cases} E_{H_i} - b \cdot E_{WS} \geq 0 \\ b \geq 0 \end{cases} \tag{12}$$

This optimization problem maximizes the amount of data, b (an integer) that each node in a measurement cycle can transmit. Using the energy harvested by node i, the energy level of the node is updated at the beginning of the following cycle as follows:

$$E_{H_i} \leftarrow\!\!\rightarrow E_{H_i} - b^* \cdot E_{WS} + \int_{t}^{t+\tau} (p_{real}(u) - p_{PHPV}(u)) \cdot du \tag{13}$$

where $p_{real}(u)$ is the actual power harvested during the earlier cycle, b^* is the solution of the optimization problem P1 defined by Equations (11) and (12), with the other parameters being defined as previously.

The protocol thus presented aimed to maximize the amount of the data transferred by the WS based on the energy expected to be collected; it was referred to in [7] as the Maximization Data Size Protocol (MDSP). However, the study only focused on a single node (the one with the highest harvest rate), thus not guaranteeing the energy autonomy of the WSN. A more generic flowchart than that proposed in [7] of the MDSP is shown in Figure 11. For an energy cost E_{WS} per data bit, the maximum and minimum size of data transferable per measurement cycle was defined, and the residual energy of each node was updated before the start of the next cycle. $N\tau$ in the flowchart represents the total number of measurement cycles; b_{min} is the minimum size of the data associated with a minimum required QoS.

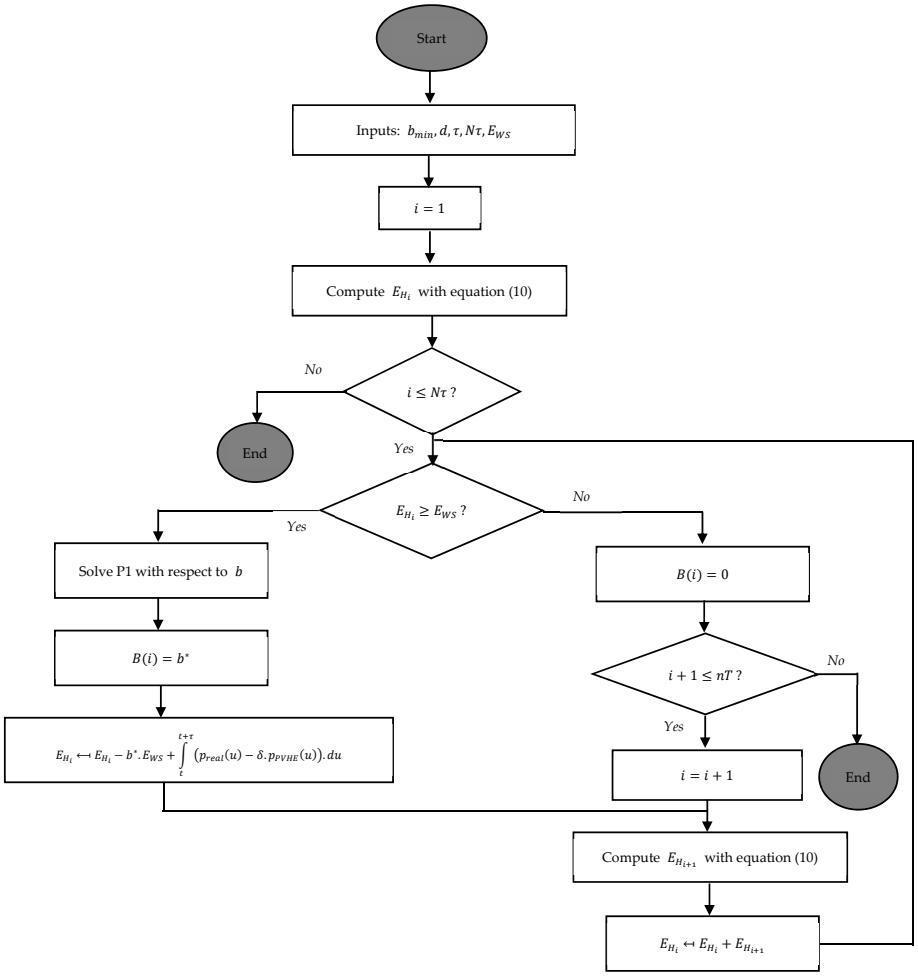

Figure 11. MDSP flowchart.

In this work, the energy cost associated with b data bits $E_{WS}\ (b,d)$ is the sum of the energy dissipation for data acquisition $E_{\text{acqui}}(b)$, for data reception $E_{rx}\ (b)$, for their processing $E_{\text{pro}}(b)$, and finally for their transmission to the BS, $E_{\text{tx}}(b,d)$ [52]. With d representing the distance between the BS and the network, it was assumed that the BS is sufficiently far from the network so that all the WSs are approximately at the same distance d from it. It was also assumed that each node has a LoRa (Long Range) transmitter, one of the IoT protocols offering advantages in terms of lifetime and capacity [53]. Many recent studies have been proposed to quantify the WS energy budget. From the review proposed in [54], it emerges that some of the most relevant results in the field have come from the work [31,52]. The different sources of dissipation considered above are then expressed as in works [7,31,52,55] by the set of Equation (14).

$$\begin{cases} E_{\text{acqui}}(b) = b{\cdot}V_{\text{sup}}{\cdot}I_{\text{sens}}{\cdot}T_{\text{sens}} + \frac{b{\cdot}V_{\text{sup}}}{8}\left(I_{\text{read}}{\cdot}T_{\text{read}} + I_{\text{write}}{\cdot}T_{\text{write}}\right) \\ E_{rx}(b) = b{\cdot}\ E_{\text{elec}} \\ E_{\text{pro}}\left(b,\ N_{\text{cyc}}\right) = b{\cdot}\left(N_{\text{cyc}}{\cdot}C_{\text{avg}}{\cdot}V_{\text{sup}}^2 + V_{\text{sup}}\left(\frac{N_{\text{cyc}}}{f}\right)\left(I_0{\cdot}e^{\left(\frac{V_{\text{sup}}}{n_P{\cdot}V_t}\right)}\right)\right) \\ E_{\text{tx}}(b,d) = \left(\frac{4\pi f_{\text{LoRa}}}{c}\right)^2\left(14.25 + \text{ceil}\left(\frac{\max\left(b + 16 - 4{\cdot}\text{SF}\quad 0\right)}{4{\cdot}\text{SF}}\right)\right)\frac{S_R{\cdot}d^4{\cdot}2^{\text{SF}}}{BW} \end{cases} \tag{14}$$

The descriptions and the values of the different estimation parameters used in these equations are provided in Table 3. These values were extracted from the datasheets of the real components and have been used in several previous research works [7,31,52,55].

Table 3. Description and parameter values for assessing the energy cost of the WS [31,52,55,56].

Symbol	Description	Value
V_{sup}	Supply Voltage to sensor	2.7 V
I_{sens}	Current sensing activity	25 mA
T_{sens}	Time duration: sensor node sensing	0.5 ms
I_{read}	Current: flash reading 1 byte data	6.2 mA
T_{read}	Time duration: flash reading	565 µs
I_{write}	Current: flash writing 1 byte data	18.4 mA
T_{write}	Time duration: flash writing	12.9 mS
E_{elec}	Energy dissipation electronics	50 nJ/bit
N_{cyc}	Number of clock cycles per task	0.97×10^6
C_{avg}	Avg. capacitance switch per cycle	22 pF
I_0	Leakage Current	1.196 mA
n_P	Constant: depending on the processor	21.26
f	Sensor frequency	191.42 MHz
V_t	Thermal voltage	0.2 V
f_{LoRa}	LoRa transmitter/receiver frequency	2.4 GHz
S_R	LoRa SX1280 transceiver sensitivity	−99 dBm
SF	Spreading factor	5
BW	Bandwidth	1625 kHz
d	Distance from WS to Base station	500 m

Assuming as in [7] that each WS transmits its data directly to the BS, the energy cost associated with the transmission of b bit of data is then defined as follows:

$$E_{WS}(b,d) = E_{\text{acqui}}(b) + E_{pro}(b) + E_{tx}(b,d) \tag{15}$$

where $E_{\text{acqui}}(b)$, $E_{pro}(b)$ and $E_{tx}(b,d)$, are defined as in the set of Equation (14). A comparison of the achieved performance as a function of the required QoS is shown in Figure 12. In these figures, B_i represents the quantity of data transmitted by node i. Table A1 of Appendix A also provides the terminology for the different positions. The minimum QoS is defined as the size b_{min} of the transmissible data.

- Figure 12a shows the evolution of each node's quantity of transmitted data during 31 days when the data size is set to 512 bits. It was observed that some WSs cannot transmit information on the state of the system because of the QoS requirement. This would make decision-making difficult, particularly for predictive maintenance operations in which the interventions consider the simultaneous observation of several data about the controlled system.
- Figure 12b shows the total amount of data transmitted by each WS during the month. It can be observed that the hierarchy observed in the harvest rate is respected. The node with the highest harvest rate transmits up to 10 kbits of data during the month.
- For Figure 12c,d, the QoS was set to 4096 bits of data, and it is observed that only 8 WS out of the 12 deployed are capable of transmitting data on the state of the system. It was also obtained that the total amount of transmitted data by each WS was greater than the case in Figure 12a,b, for which the data size was set at 512 bits. For example, the WS with a higher harvest rate transmits up to 80 kbits during the month instead of 10 kbits transferred when the data size is set at 512 bits.
- For Figure 12e,f, a variable data size between 128 and 4096 bits was assumed. It was observed that overall, the total quantity of data transmitted by each of the WSs had increased. However, the WS with the highest harvest rate is not the one that sends the most long-term data. This is explained by the fact that it exhausts its energy reserve at the start of the cycle while the other WSs accumulate enough energy to be then able to transmit large quantities of data.

Overall, the results of Figure 12 show that it would be difficult to completely control the industrial process studied here using WS powered by energy harvested from vibrations. Even by minimizing the data size, some nodes will not be able to transmit enough information given their harvesting capacity. This makes it challenging to implement a vibratory energy harvester WSN without an external energy supply to some WSs. We overcame this limitation in the following subsection by proposing the Hierarchical Energy-Balancing Protocol (HEBP).

4.3. Optimizing WSN Performance with HEBP

4.3.1. Conceptual View

The results of the previous subsection highlighted the heterogeneous nature of an ambient energy harvester WSN. Considering that the harvest rates of the different WS are not equal, we envisaged in the protocol proposed here to define a hierarchy of the various WSs of the network at the beginning of each measurement cycle. The WS ranking was established based on each node's energy level at the start of the cycle. At the start of the nth measurement cycle, the energy level E_{i_n} of a node i was evaluated as follows:

$$E_{i_n} = E_{H_{i_n}} + E_{R_{i_{n-1}}} \tag{16}$$

where $E_{H_{i_n}}$ is the energy predicted by the PHPV evaluated by Equation (10) and $E_{R_{i_{n-1}}}$ is the residual energy at the end of the previous cycle, and this is evaluated with Equation (13).

The energy cost associated with the minimum required QoS (b_{min}) is designated by E_{min}. Three categories of WS are defined based on the energy levels defined above. The node with the highest energy level is the CH, WSs with an energy level below E_{min} are classified as the needy nodes, while WSs with an energy greater than E_{min} are self-sufficient nodes. A hierarchy was then established between these other two categories of WSs:

- For the needy WSs, the classification is made from the least needy to the neediest.
- Self-sufficient WSs are classified from most self-sufficient to least self-sufficient.

Once this hierarchy was established, it was then carried out to balance the energy of the different WSs. In the protocol, the self-sufficient WS with the highest energy will start delivering its extra energy to the needy node with the lowest energy deficit and so on. This will maximize the number of WSs that can transmit during a measurement cycle. Once this balancing is achieved, all nodes will send data, avoiding long queues in data memory for

needy WSs. The protocol proposed to ensure this minimum QoS to the network is called the Hierarchical Energy Balancing Protocol (HEBP). The operating algorithm boils down to the different steps shown on the block diagram in Figure 13.

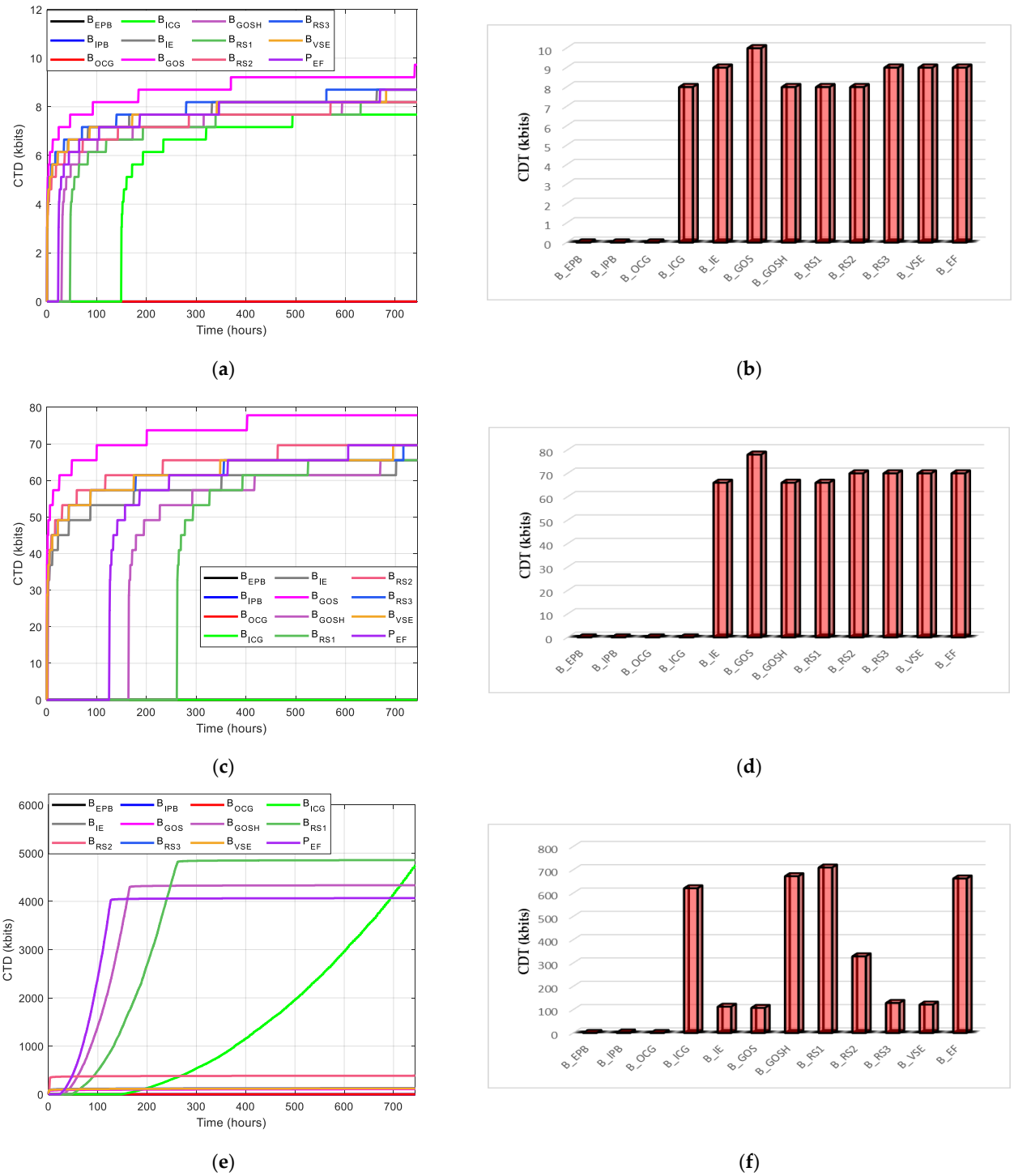

Figure 12. Performances DSMP. (**a**) Cumulated transmitted data for $b_{min} = 512$ bits. (**b**) Quantity of data transmitted by each node during the month for $b_{min} = 512$ bits. (**c**) Cumulated transmitted data for $b_{min} = 4096$ bits. (**d**) Quantity of data transmitted by each node during the month for $b_{min} = 4096$ bits. (**e**) Cumulated transmitted data for 512 bits $\leq b_{min} \leq 4096$ bits. (**f**) Quantity of data transmitted by each node during the month for 128 bits $\leq b_{min} \leq 4096$ bits.

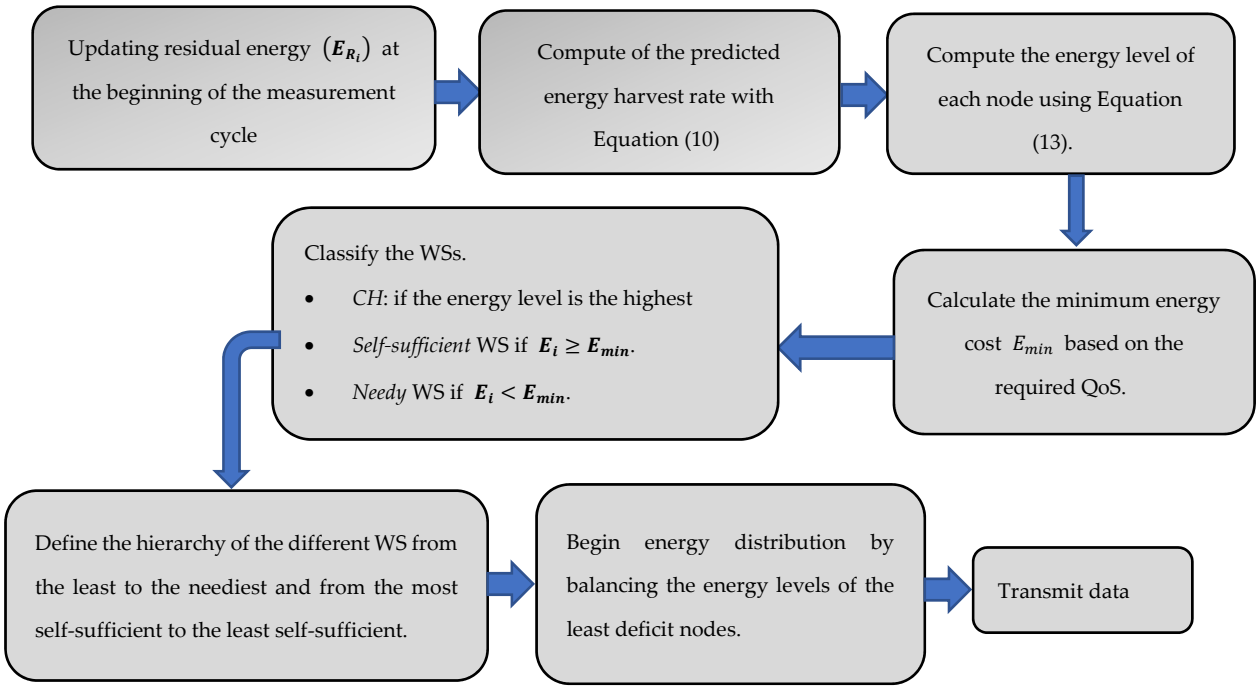

Figure 13. HEBP design stage.

Unlike the MDSP, whose performance was evaluated in the previous subsection, each node transmits its data to the cluster head, thus reducing the energy dissipation associated with long-range transmission to the BS. The free space model was used to fill the energy gap of a needy WS as in [57]. Thus, the energy E_t transmitted by the self-sufficient WS to a needy WS was defined as follows, assuming unity antenna gains:

$$E_t = E_r \left(\frac{4\pi f_{\text{LoRa}} d_1}{c} \right)^2 \quad (17)$$

where $c = 3 \times 10^8$ m/s is the speed of light, f_{LoRa} is the frequency of the LoRa transmitter, and d_1 is a distance between the self-sufficient WS and the needy WS fixed at 10 m, corresponding to the average dimensions of the semi-autogenous mill [58]. E_r is the energy received by the needy WS; it was evaluated as the energy gap between the energy level E_i of the WS and the energy E_{min} required to satisfy the minimum QoS. It was then calculated as follows:

$$E_r = E_{min} - E_i \quad (18)$$

4.3.2. HEBP Performance

The performance of HEBP compared to that of DSMP, the previously considered protocol for WS powered by an energy harvesting process, is shown in Figure 14.

- In Figure 14a, we observed for a data size set of 512 bits that each WS transmits up to 23 Mbits of data, unlike the at-most 10 kbits of data as shown in Figure 12b.
- In Figure 14b, the data size is set to 1024 bits, and it was observed that the maximum data size had doubled; each WS transmitted up to more than 45 Mbits of data.
- Figure 14c compares the performances achieved in the case of DSMP and HEBP; this was for a variable data size between 512 and 4096 bits. It was first observed that all the WSs of the network transmit information, unlike the result obtained with the DSMP, where only 5 of the 12 WSs could communicate.
- Figure 14d shows the effective range of HEBP; for this, the number of active WSs for each protocol is compared as a function of the data size. It shows that with HEBP, the 12 WSs deployed on the system transmit data when the data size is less than 1100 bits.

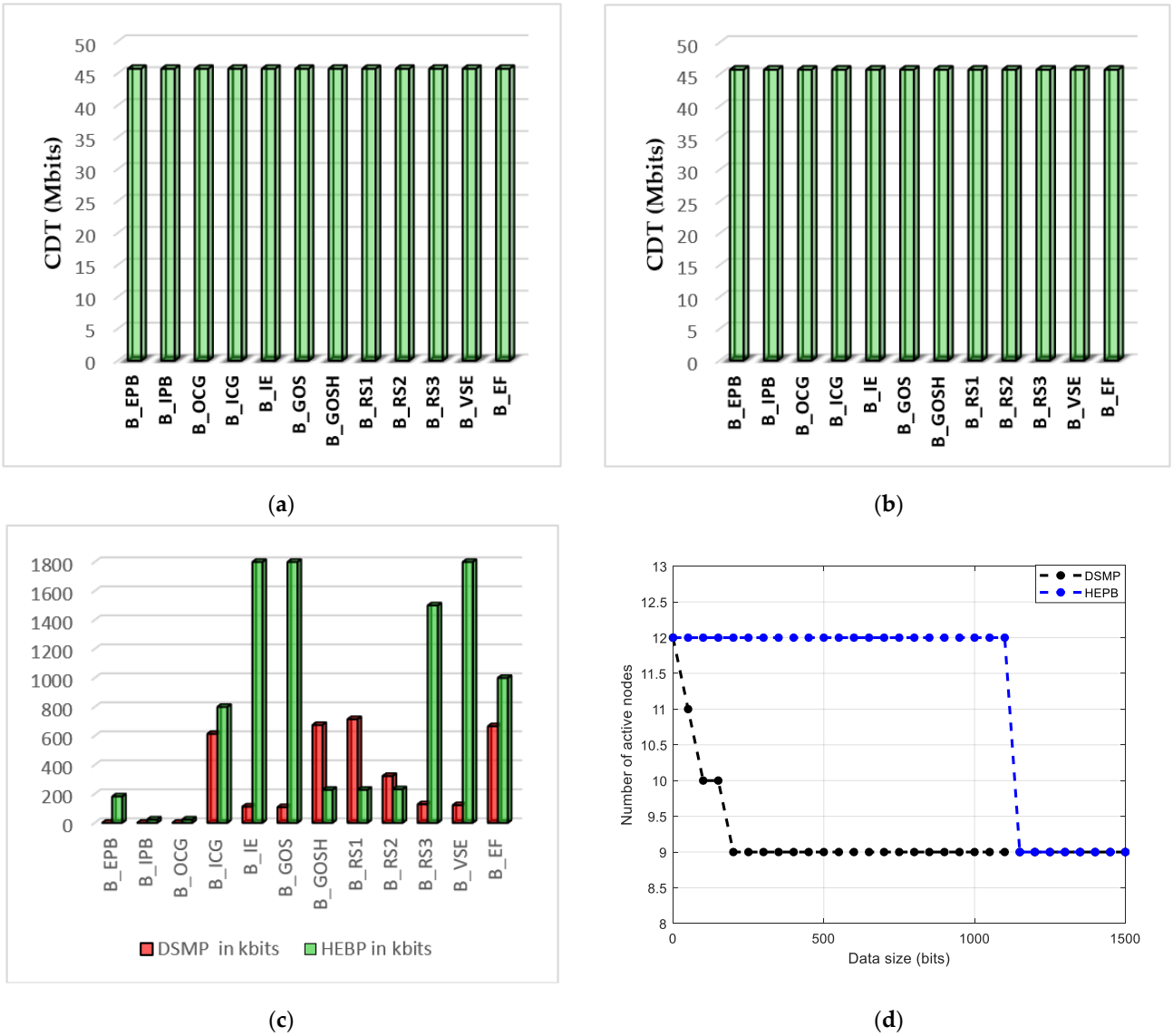

Figure 14. Comparison of HEPB performance with DSMP. (**a**) $b = 512$ bits. (**b**) $b = 1024$ bits. (**c**) $b \in \left[128 \text{ bits}, \quad 4096 \text{ bits}\right]$. (**d**) HEBP efficiency range.

5. Conclusions and Prospects

In this paper, a new method to ensure the energy autonomy of a WSN has been proposed. It was a question of first setting up the PHPV to predict the amount of energy harvestable by each WSs. The predictor's performance was compared with that of the previous predictor, the PHEV and the EWMA, which are widely used. The industrial process, of the drive diagram of a mill at the Laronde mine has been described (types and location of the various sensors). Vibration data was recorded for 31 days at 12 different locations on the process, with a sample taken every minute. To minimize prediction errors while saving data storage space, PHPV exploited the correlation between the predicted power and that measured at the preceding period during the day and at the same period of the earlier day. Compared to the PHEV predictor, PHPV improved the RMSE from 37.2 to 78.32%.

Based on the possibility of estimating the energy level of each WSs deployed in the process, a solution was implemented to better manage the entire wireless sensor network's energy. The objective of the method was to maximize the number of WSs that can communicate in a measurement cycle by promoting energy assistance between

the different WS. A minimum QoS was set, and a hierarchy was established between the different WSs. The HEBP was then set up to balance the energy level of the various WSs in the network to allow each of the WSs to communicate information during each measurement cycle. This new protocol allowed up to 100% of the WSs deployed on the system to communicate, compared to only 66% with previous protocols. Overall, the proposed method makes it possible to ensure the energy autonomy of a WSN and not of a single WS, as is the case in most studies. Note, however, that the performance achieved here may be affected during practical implementation by factors such as the dynamic nature of the channel between a needy WS and a self-sufficient WS as well as by losses in the energy-harvested shaping circuit.

Author Contributions: Idea, A.M.; Conceptualization, A.M.; methodology, A.M. and H.M.; Data Acquisition, H.M.; Mechanical-electric conversion A.M. and H.M.; Predictor of the Harvestable Energy from vibrations, A.M. and H.M.; Hierarchical Energy-Balancing Protocol, A.M.; writing—original draft preparation, A.M.; writing—review and editing, H.M.; supervision, H.M. All authors have read and agreed to the published version of the manuscript.

Funding: This research was funded by Mitacs Canada, funder number: IT26434.

Institutional Review Board Statement: Not applicable.

Informed Consent Statement: Not applicable.

Data Availability Statement: Not applicable.

Conflicts of Interest: The authors declare no conflict of interest.

Appendix A

Table A1. Nomenclature of different sensors and measurements.

Name of Sensors	Corresponding Acceleration	Corresponding Harvested Power/Harvested Energy/Transmitted Data	Description
V_{EPB}	A_{EPB}	$P_{ECP}/E_{ECP}/B_{ECP}$	External Crusher Pinion vibration
V_{IPB}	A_{IPB}	$P_{ICP}/E_{ICP}/B_{ICP}$	Inside Crusher Pinion vibration
V_{OCG}	A_{OCG}	$P_{OCG}/E_{OCG}/B_{OCG}$	Vibration at the Outlet of the Crusher Gearbox.
V_{ICG}	A_{ICG}	$P_{ICG}/E_{ICG}/B_{ICG}$	Vibration at the Inlet of the Crusher Gearbox
V_{IE}	A_{IE}	$P_{IE}/E_{IE}/B_{IE}$	Internal Engine vibration
V_{GOS}	A_{GOS}	$P_{GOS}/E_{GOS}/B_{GOS}$	Vibration on the Gearbox at the Output Side
V_{GOSH}	A_{GOSH}	$P_{GOSH}/E_{GOSH}/B_{GOSH}$	Vibration on the Gearbox Output SHaft
V_{RS1}	A_{RS1}	$P_{RS1}/E_{RS1}/B_{RS1}$	Vibration at Radial Shaft 1
V_{RS2}	A_{RS2}	$P_{RS2}/E_{RS2}/B_{RS2}$	Vibration Radial Shaft 2
V_{RS3}	A_{RS3}	$P_{RS3}/E_{RS3}/B_{RS3}$	Vibration Radial Shaft 3
V_{VSE}	A_{VSE}	$P_{VSE}/E_{VSE}/B_{VSE}$	Vibration on the Ventilation Side of the Engine
V_{EF}	A_{EF}	$P_{EF}/E_{EF}/B_{EF}$	Engine Fan vibration

References

1. Guo, Y.; Wang, N.; Xu, Z.-Y.; Wu, K. The internet of things-based decision support system for information processing in intelligent manufacturing using data mining technology. *Mech. Syst. Signal Process.* **2020**, *142*, 106630.
2. Zhang, S.; Zhang, H. A review of wireless sensor networks and its applications. In Proceedings of the 2012 IEEE International Conference on Automation and Logistics, Zhengzhou, China, 15–17 August 2012; pp. 386–389.
3. Rehman, M.A.U.; Ullah, R.; Park, C.-W.; Kim, B.S. Towards network lifetime enhancement of resource constrained iot devices in heterogeneous wireless sensor networks. *Sensors* **2020**, *20*, 4156.
4. Mishu, M.K.; Rokonuzzaman, M.; Pasupuleti, J.; Shakeri, M.; Rahman, K.S.; Hamid, F.A.; Tiong, S.K.; Amin, N. Prospective efficient ambient energy harvesting sources for iot-equipped sensor applications. *Electronics* **2020**, *9*, 1345.
5. Lefeuvre, E.; Badel, A.; Richard, C.; Guyomar, D. Energy harvesting using piezoelectric materials: Case of random vibrations. *J. Electroceram.* **2007**, *19*, 349–355.
6. Bacci di Capaci, R.; Scali, C. A cloud-based monitoring system for performance assessment of industrial plants. *Ind. Eng. Chem. Res.* **2020**, *59*, 2341–2352.

7. Mouapi, A.; Hakem, N.; Kandil, N. Piezoelectric Energy Harvesting Prediction and Efficient Management for Industrial Wireless Sensor. *Appl. Sci.* **2020**, *10*, 8486.
8. Basaran, S. Hybrid energy harvesting system under the electromagnetic induced vibrations with non-rigid ground connection. *Mech. Syst. Signal Process.* **2022**, *163*, 108198.
9. Abou-Rjeily, C.; Kaddoum, G. Free space optical cooperative communications via an energy harvesting harvest-store-use relay. *IEEE Trans. Wirel. Commun.* **2020**, *19*, 6564–6577.
10. Beeby, S.P.; Tudor, M.J.; White, N. Energy harvesting vibration sources for microsystems applications. *Meas. Sci. Technol.* **2006**, *17*, R175.
11. Ahmad, I.; Hee, L.M.; Abdelrhman, A.M.; Imam, S.A.; Leong, M.S. Scopes, challenges and approaches of energy harvesting for wireless sensor nodes in machine condition monitoring systems: A review. *Measurement* **2021**, *183*, 109856.
12. Roundy, S.; Wright, P.K. A piezoelectric vibration based generator for wireless electronics. *Smart Mater. Struct.* **2004**, *13*, 1131.
13. Roundy, S.; Wright, P.K.; Rabaey, J. A study of low level vibrations as a power source for wireless sensor nodes. *Comput. Commun.* **2003**, *26*, 1131–1144.
14. Mouapi, A.; Hakem, N.; Kandil, N. Cantilevered piezoelectric micro generator design issues and application to the mining locomotive. *Energies* **2019**, *13*, 63.
15. Mouapi, A. Piezoelectric micro generator design and characterization for self-supplying industrial wireless sensor node. *Mem.-Mater. Devices Circuits Syst.* **2022**, *1*, 100002. [CrossRef]
16. Lan, C.; Chen, Z.; Hu, G.; Liao, Y.; Qin, W. Achieve frequency-self-tracking energy harvesting using a passively adaptive cantilever beam. *Mech. Syst. Signal Process.* **2021**, *156*, 107672.
17. Caliò, R.; Rongala, U.B.; Camboni, D.; Milazzo, M.; Stefanini, C.; De Petris, G.; Oddo, C.M. Piezoelectric energy harvesting solutions. *Sensors* **2014**, *14*, 4755–4790.
18. Yu, H.; Zhou, J.; Deng, L.; Wen, Z. A vibration-based MEMS piezoelectric energy harvester and power conditioning circuit. *Sensors* **2014**, *14*, 3323–3341.
19. Shi, G.; Xia, Y.; Yang, Y.; Chen, J.; Peng, Y.; Xia, H.; Wang, X.; Qian, L. A Sensor-less Self-tuning Resonance System for Piezoelectric Broadband Vibration Energy Harvesting. *IEEE Trans. Ind. Electron.* **2020**, *68*, 2225–2235.
20. Del-Rio-Ruiz, R.; Echevarria, J.J.; Eguiluz, X.; Lopez-Garde, J.-M.; Legarda, J. Experimental Frequency Tuning Methodology of a Cantilever Piezoelectric Harvester Validated in a Multimodal Transportation. *Electronics* **2020**, *9*, 79.
21. Asanuma, H.; Komatsuzaki, T. Nonlinear piezoelectricity and damping in partially-covered piezoelectric cantilever with self-sensing synchronized switch damping on inductor circuit. *Mech. Syst. Signal Process.* **2020**, *144*, 106867.
22. Liang, J.; Liao, W.-H. Improved design and analysis of self-powered synchronized switch interface circuit for piezoelectric energy harvesting systems. *IEEE Trans. Ind. Electron.* **2011**, *59*, 1950–1960.
23. Li, Z.; Chen, Z.; Wan, Q.; Kuai, Q.; Liang, J.; Mok, P.K.; Zeng, X. An Energy Harvesting System with Reconfigurable Piezoelectric Energy Harvester Array for IoT Applications. In Proceedings of the 2020 IEEE International Symposium on Circuits and Systems (ISCAS), Seville, Spain, 12–14 October 2020; pp. 1–5.
24. Kassan, S.; Gaber, J.; Lorenz, P. Autonomous energy management system achieving piezoelectric energy harvesting in wireless sensors. *Mob. Netw. Appl.* **2020**, *25*, 794–805.
25. Han, Y.; Feng, Y.; Yu, Z.; Lou, W.; Liu, H. A study on piezoelectric energy-harvesting wireless sensor networks deployed in a weak vibration environment. *IEEE Sens. J.* **2017**, *17*, 6770–6777.
26. Liu, X.; Liu, A.; Wang, T.; Ota, K.; Dong, M.; Liu, Y.; Cai, Z. Adaptive data and verified message disjoint security routing for gathering big data in energy harvesting networks. *J. Parallel Distrib. Comput.* **2020**, *135*, 140–155.
27. Ma, Y.; Ji, Q.; Chen, S.; Song, G. An experimental study of ultra-low power wireless sensor-based autonomous energy harvesting system. *J. Renew. Sustain. Energy* **2017**, *9*, 054702.
28. Ren, Q.; Yao, G. An energy-efficient cluster head selection scheme for energy-harvesting wireless sensor networks. *Sensors* **2020**, *20*, 187.
29. Sah, D.K.; Amgoth, T. A novel efficient clustering protocol for energy harvesting in wireless sensor networks. *Wirel. Netw.* **2020**, *26*, 4723–4737.
30. Sah, D.K.; Amgoth, T. Renewable Energy Harvesting Schemes in Wireless Sensor Networks: A Survey. *Inf. Fusion* **2020**, *63*, 223–247.
31. Heinzelman, W.B.; Chandrakasan, A.P.; Balakrishnan, H. An application-specific protocol architecture for wireless microsensor networks. *IEEE Trans. Wirel. Commun.* **2002**, *1*, 660–670.
32. Radhika, M.; Sivakumar, P. Energy optimized micro genetic algorithm based LEACH protocol for WSN. *Wirel. Netw.* **2020**, *27*, 27–40.
33. Han, B.; Ran, F.; Li, J.; Yan, L.; Shen, H.; Li, A. A Novel Adaptive Cluster Based Routing Protocol for Energy-Harvesting Wireless Sensor Networks. *Sensors* **2022**, *22*, 1564. [PubMed]
34. Engineering, O. ACC101, ACC102A, ACC103, ACC301A, ACC310, ACC320 Accelerometers. Available online: https://assets.omega.com/manuals/M5097.pdf (accessed on 15 March 2020).
35. Srikanth, K.V.A.K. State of art: Piezoelectric vibration energy harvesters. *Mater. Today Proc.* **2017**, *4*, 1091–1098.
36. Ibrahim, H.H.; Singh, M.S.; Al-Bawri, S.S.; Islam, M.T. Synthesis, Characterization and Development of Energy Harvesting Techniques Incorporated with Antennas: A Review Study. *Sensors* **2020**, *20*, 2772.

37. Yang, F.; Du, L.; Yu, H.; Huang, P. Magnetic and Electric Energy Harvesting Technologies in Power Grids: A Review. *Sensors* **2020**, *20*, 1496.
38. Newbury, K.M.; Leo, D.J. Linear electromechanical model of ionic polymer transducers-Part I: Model Development. *J. Intell. Mater. Syst. Struct.* **2003**, *14*, 333–342.
39. Saraereh, O.A.; Alsaraira, A.; Khan, I.; Choi, B.J. A hybrid energy harvesting design for on-body Internet-of-Things (IoT) networks. *Sensors* **2020**, *20*, 407.
40. He, S.; Tang, Y.; Li, Z.; Li, F.; Xie, K.; Kim, H.-J.; Kim, G.-J. Interference-aware routing for difficult wireless sensor network environment with SWIPT. *Sensors* **2019**, *19*, 3978.
41. Mathworks. Piezo Stack. Available online: https://www.mathworks.com/help/physmod/elec/ref/piezostack.html (accessed on 18 May 2020).
42. MIDE. QuickPack Packaged Piezoelectric Actuators and Sensors. Available online: https://www.mouser.com/datasheet/2/606/mide%20technology_quickpack-actuator-sensor-datashee-1214998.pdf (accessed on 30 March 2018).
43. Piorno, J.R.; Bergonzini, C.; Atienza, D.; Rosing, T.S. Prediction and management in energy harvested wireless sensor nodes. In Proceedings of the 2009 1st International Conference on Wireless Communication, Vehicular Technology, Information Theory and Aerospace & Electronic Systems Technology, Aalborg, Denmark, 17–20 May 2009; pp. 6–10.
44. Bouguera, T.; Diouris, J.-F.; Andrieux, G.; Chaillout, J.-J.; Jaouadi, R. A novel solar energy predictor for communicating sensors. *IET Commun.* **2018**, *12*, 2145–2149.
45. Kansal, A.; Hsu, J.; Zahedi, S.; Srivastava, M.B. Power management in energy harvesting sensor networks. *ACM Trans. Embed. Comput. Syst.* **2007**, *6*, 32-es.
46. Zhang, C.; Hu, G.; Yurchenko, D.; Lin, P.; Gu, S.; Song, D.; Peng, H.; Wang, J. Machine learning based prediction of piezoelectric energy harvesting from wake galloping. *Mech. Syst. Signal Process.* **2021**, *160*, 107876.
47. Cox, D.R. Prediction by exponentially weighted moving averages and related methods. *J. R. Stat. Soc. Ser. B* **1961**, *23*, 414–422.
48. Wang, S.; Zhu, R.; Xiao, Z. Investigation on crack failure of helical gear system of the gearbox in wind turbine: Mesh stiffness calculation and vibration characteristics recognition. *Ocean Eng.* **2022**, *250*, 110972.
49. Martínez, J.-F.; Garcí, A.-B.; Corredor, I.; López, L.; Hernández, V.; Dasilva, A. QoS in wireless sensor networks: Survey and approach. In Proceedings of the 2007 Euro American Conference on Telematics and Information Systems, Faro, Portugal, 14–17 May 2007; pp. 1–8.
50. Siddiqui, A.M.; Musavian, L.; Ni, Q. Energy efficiency optimization with energy harvesting using harvest-use approach. In Proceedings of the 2015 IEEE International Conference on Communication Workshop (ICCW), London, UK, 8–12 June 2015; pp. 1982–1987.
51. Wang, H.; Zhou, G.; Bhatia, L.; Zhu, Z.; Li, W.; McCann, J.A. Energy-Neutral and QoS-Aware Protocol in Wireless Sensor Networks for Health Monitoring of Hoisting Systems. *IEEE Trans. Ind. Inform.* **2020**, *16*, 5543–5553.
52. Halgamuge, M.N.; Zukerman, M.; Ramamohanarao, K.; Vu, H.L. An estimation of sensor energy consumption. *Prog. Electromagn. Res. B* **2009**, *12*, 259–295.
53. Mekki, K.; Bajic, E.; Chaxel, F.; Meyer, F. A comparative study of LPWAN technologies for large-scale IoT deployment. *ICT Express* **2019**, *5*, 1–7.
54. Roy, N.R.; Chandra, P. Energy dissipation model for wireless sensor networks: A survey. *Int. J. Inf. Technol.* **2019**, *12*, 1343–1353.
55. Semtech. SX1280/SX1281 Long Range, Low Power, 2.4 GHz Transceiver with Ranging Capability. Available online: https://semtech.my.salesforce.com/sfc/p/E0000000JelG/a/2R000000HoCW/8EVYKPLcthcKCB_cKzApAc6Xf6tAHtn9.UKcOh7SNmg?__hstc=212684107.a2777854172938a3600e24e6b3622154.1640973435576.1640973435576.1640973435576.1&__hssc=212684107.1.1640973435577&__hsfp=3233074646 (accessed on 12 October 2021).
56. Choudhary, P.; Bhargava, L.; Singh, V.; Choudhary, M.; Kumar Suhag, A. A survey–Energy harvesting sources and techniques for internet of things devices. *Mater. Today Proc.* **2020**, *30*, 52–56.
57. Schott, L.; Fromm, R.; Bouattour, G.; Kanoun, O.; Derbel, F. Analytical and Experimental Performance Analysis of Enhanced Wake-Up Receivers Based on Low-Power Base-Band Amplifiers. *Sensors* **2022**, *22*, 2169.
58. Orser. CONGA: THE WORLD'S FIRST 42 FOOT DIAMETER 28 MW GEARLESS SAG MILL. Available online: https://library.e.abb.com/public/e23fc5fb2ee49033c125793d0056bce5/CONGA%20-%20THE%20WORLDS%20FIRST%2042%20FOOT%20DIAMETER%2028%20MW%20GEARLESS%20SAG%20MILL.pdf (accessed on 15 March 2022).